Structural Chemistry
https://doi.org/10.1007/s11224-026-02834-1

RESEARCH

Polymorphism and structural diversity in calix[*n*]arenes (*n* = 4, 6 or 8)

Marcelo Augusto Moraes da Luz[1] · Meiry Edivirges Alvarenga[1] · Bárbara Júlia Gonçalves Dutra[1] · Guilherme Martins Fernandes[2] · Freddy Fernandes Guimarães[1] · Ângelo de Fátima[2,3] · Cleiton Moreira da Silva[2] · Felipe Terra Martins[4]

Received: 22 April 2026 / Accepted: 16 June 2026

Abstract

This paper reports six crystal structures of five calix[*n*]arenes (*n* = 4, 6, or 8), highlighting the remarkable ability of this molecular class to self-assemble into diverse architectures and conformations, and rationalizing which structural features predispose calixarenes to act as supramolecular hosts. The structures of *p*-sulfonatocalix[4]arene and 1,3-bis(carboxymethyl)calix[4]arene reveal open-crown conformations accessible to guest molecules, both in the calcium salt and DMSO solvate forms, respectively. Closed-crown conformations were identified in two conformational polymorphs of hexakis(carboxymethyl)calix[6]arene methyl ester and in a lower-rim *n*-butyl-functionalized *p-tert*-butylcalix[8]arene derivative, in which their first crystal structures are reported here. Meanwhile, the *p-tert*-butylcalix[8]arene without lower-rim functionalization crystallizes with two structurally similar pleated-loop conformers that display distinct packing motifs. Hirshfeld surface analyses and DFT help us also to understand the interactions patterns and conformerism, such as the finding of an atypical high-energy 1,2,3-alternate conformer in which the closed crown is kept by π···π interactions between phenyl rings in one of the two polymorphs of hexakis(carboxymethyl)calix[6]arene methyl ester.

Keywords Crystal structure · Calixarene · Polymorphism · DFT · Hirshfeld surface · Crystal packing

Introduction

Calixarenes are heterocyclic compounds made up of phenolic units cross linked by methylene bridges at 2,6-positions. They have been widely explored as molecular carriers due to their ability to assemble host-guest inclusion supramolecular entities, that is, stable aggregates comprising different molecules kept in contact through non-covalent interactions [1–5].

This ability emerges from the hydrophobic pocket formed inside the crown that encloses the guest compound and that names the compound class. Nevertheless, some calixarenes had served as cocrystallization platforms in the solid state without direct inclusion of the target drug molecule within the crown [6], so the inclusion of guest solvent is necessary to cocrystal formation with other larger compounds [7].

It is well known that both functionalization of the upper rims (crown top) and the lower rims (hydroxyl groups) drive the properties of calixarene, including their propensity to act as molecular hosts, since these groups can establish further interactions with guests or lead to a specific conformation suitable for inclusion or not [8–12]. Furthermore, functionalization of the rims dictates solvatomorphism and polymorphism. For instance, substituted *p-tert*-butylthiacalix [4]arenes have been well investigated in terms of multiple crystal forms [13–15]. One of them is the *p-tert*-butylthiacalix [4]arene tetrasubstituted with ethylcarboxymethyl groups on the lower rim, which presents different crystal forms due to conformational mobility of its substituents [13]. More related to this study, true polymorphism is reported in tetrakis(carboxymethyl)calix [4]arene

✉ Felipe Terra Martins
felipe.martins@unifal-mg.edu.br

1 Instituto de Química, Universidade Federal de Goiás, Goiania, GO 74001-970, Brazil

2 Departamento de Química, Instituto de Ciências Exatas, Universidade Federal de Minas Gerais, Belo Horizonte, MG 31270-901, Brazil

3 Department of Organic Chemistry, Faculty of Science, Atatürk University, Erzurum 25240, Türkiye

4 Instituto de Química, Universidade Federal de Alfenas, Alfenas, MG 37130-001, Brazil

Published online: 19 June 2026

methyl ester, which only differs for the number of calix[*n*] arene units from one of the compounds studied here (*n* = 4 in the literature compound and 6 in compound 3, see below). It is known to crystallize in different crystal forms without cocrystallized solvent molecule, adopting either cone-shaped or 1,3-alternate conformations [16].

Here, we report six crystal structures of five calix[*n*] arenes (*n* = 4, 6 or 8; compounds 1–5 in Table 1), showing the structural diversity in this molecular class and how the number of units and the substitution pattern affect their conformation. Closed crown is found in two polymorphs of one calix [6]arene (compound 3) and in one calix [8]arene (compound 4), while the crown remains open to guest molecules in two calix [4]arenes (compounds 1 and 2) and in another calix [8]arene unsubstituted at lower rim (compound 5). Hirshfeld surface analyzes were employed to depict interactions patterns of the calixarene structures, and the found polymorphs were also investigated by electronic structure calculations based on density functional theory (DFT).

Experimental

Synthesis

Compounds 2, 4, and 5 were obtained according to previously published methodologies [17, 18]. Full synthetic procedures and characterization data, including infrared spectroscopy and ^{1}H and ^{13}C nuclear magnetic resonance, for compounds 1 and 3 are detailed in the Supplementary Material.

Single crystal X-ray diffraction

Single crystals of suitable size were obtained from room temperature slow solvent evaporation from the following solutions (5 mL) loading 5 mg of the corresponding calix[*n*] arene: DMSO (1), ethyl alcohol (2, where 1 mg of $CaCl_2$ was also dissolved together with the target compound, and 3 – Form I), methyl alcohol (3 – Form II), and toluene (4 and 5). Crystal formation occurred within around 5 days, except for 1 (around one month). Single crystals were selected for the collection of X-ray diffraction data using a Bruker diffractometer equipped with an APEX II CCD detector at 293 K. Cell refinement was performed with the APEX III programs, while the raw data set treatment was performed with the SAINT and SADABS programs [19]. The structures were solved and refined by SHELX [20] using OLEX2 systems [21], and all non-hydrogen atoms were refined with anisotropic thermal parameters. CH Hydrogens were added to their bonded atoms and constrained during refinements following a riding model with unchanged bond angles and lengths (0.93 Å, 0.96 Å and 0.97 Å in the Csp^2, methyl and methylene groups, respectively). OH Hydrogens were found from the difference Fourier electronic density map, and their positional parameters also were constrained during refinements with standard bond lengths (0.82 Å, or 0.85 Å in water). The isotropic thermal parameters of hydrogens were set to 1.2 times the Ueq of the bonded carbon (except for methyl hydrogens and OH ones, where this value was 1.5 times the Ueq of the bonded carbon or oxygen). The interpretation of the structure, including the measurement of geometric parameters and the preparation of the drawings, was performed with Mercury [22]. The complete X-ray diffraction data set for each structure, including the final refinement file and hkl data set, is available under the CCDC number codes shown in Table 2, together with a brief report of the collection and processing of the X-ray diffraction data.

Smeared electronic density peaks were also found in the difference Fourier map of 1, 4 and 5, which can be probably non-stoichiometric solvent molecules. However, their assignment was not possible and their contribution to the X-ray scattering was removed in these datasets using the solvent mask tool available in OLEX2 [21], and then not reported in their molecular formula shown in Table 2.

We have not assigned precisely the electron counting in the voids to solvent molecules because of the low amount of observed data (below 50% in the three structures,

Table 1. The calix[*n*]arenes studied here

N	Structure
1	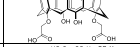
2	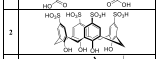
3	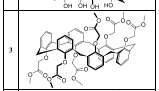
4	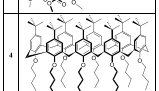
5	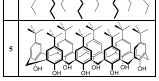

Table 2 Summary of crystal data collected with MoKα at 293 K and refinement statistics for the five structures elucidated for the first time here

	1	2	3 - Form I	3 - Form II	4	5
structural formula	$(C_{32}H_{28}O_8)$ $(C_2H_6OS)_3$	$Ca_3(C_{28}H_{21}O_{16}S_4)_2$ $(C_2H_6O)_4(H_2O)_{16}$	$C_{60}H_{60}O_{18}$	$C_{60}H_{60}O_{18}$	$C_{120}H_{176}O_8$	$C_{88}H_{112}O_8$
space group	$P2_12_12_1$	$P2_1/n$	P-1	P-1	P-1	P-1
Z/Z'	4/1	2/0.5	2/1	2/1	2/1	4/2
a (Å)	10.339(6)	10.762(3)	11.5688(19)	9.538(4)	16.827(3)	17.421(4)
b (Å)	12.52(2)	27.453(6)	12.443(2)	14.685(6)	17.200(4)	21.725(4)
c (Å)	30.86(2)	14.925(3)	20.709(3)	20.620(8)	21.879(4)	29.323(6)
α (°)	90	90	78.840(4)	84.029(9)	97.375(12)	100.621(5)
β (°)	90	96.687(6)	75.187(4)	84.816(10)	105.376(11)	104.138(5)
g (°)	90	90	72.953(4)	72.412(9)	90.438(13)	97.879(6)
V $(Å)^3$	3995(7)	4379.5(17)	2732.6(7)	2733.0(19)	6049(2)	10,382(4)
θ *r*ange for data collection (°)	1.76–25.35	1.48–25.10	1.03–25.06	1.46–25.21	1.70-25.14	0.97–25.26
Completeness to q_{max} (%)	99.7	99.7	99.6	98.7	96.4	98.3
data collected	54,494	68,525	55,809	59,382	48,245	158,212
unique reflections	7262	7768	9642	9730	20,846	37,000
unique reflections with $I>2\sigma(I)$	3570	3745	3086	3909	5957	7890
symmetry factor (R_{int})	0.1581	0.2019	0.1984	0.1287	0.1087	0.1977
parameters refined	469	578	714	703	1154	1729
goodness-of-fit on F^2	0.857	1.018	0.969	1.017	1.041	0.818
final *R1* factor for $I>2\sigma(I)$	0.0889	0.0802	0.0957	0.0847	0.2063	0.1091
wR2 factor for all data	0.2892	0.2255	0.3140	0.2449	0.5175	0.3173
largest Δρ peaks ($e/Å^3$)	1.421/-0.619	0.653/-0.612	0.537/-0.478	0.707/-0.633	1.030/-0.790	0.342/-0.276
CCDC deposit number	2,546,792	2,546,791	2,546,794	2,546,793	2,546,795	2,546,796

approximately 28% and 21% in 4 and 5). The absence of strong high-order reflections precludes the reliability of the electron count using the OLEX2 mask. Therefore, even if anyone is sure of which solvent proportion is in the void, the electron number could not be reliably attributed to solvent content on the basis of such poor intensity data from the weakly diffracting crystal. In fact, these low-order phenomena and the derived unsatisfactory refinement statistics are well known for the determination of the crystal structure of calixarenes, mainly in solvated crystal forms [23].

Finally, refinement convergence had not been full in the structure of 4 due to disorder in the alkyl tails in the lower rim which could not be modeled properly based on the poor data set as mentioned earlier. It is important to note that trial refinements were used with the split-atom approach. However, since the extra disordered sites were very close together, still higher correlation and more unstable refinements were observed by applying the classical split-atom approach to *n*-butyl. Then, to achieve full convergence, this structure was first refined using conjugate gradient least-square method (CGLS instruction), and then full matrix least-square (L.S. instruction) refinement followed.

To further compare the intermolecular interactions patterns found in the studied structures, the Hirshfeld surfaces were calculated using Crystal Explorer software (version 21.5) [24]. The surfaces were also analyzed by plotting the fingerprints made up of external distance (de, the distance between the calculated Hirshfeld surface and the nearest atom of a packed molecule outside the calculated surface) versus internal distance (di, the shortest separation from the calculated Hirshfeld surface to an atom of the molecule within the calculated surface) [25].

Quantum chemical calculations

The electronic structure calculations and molecular geometrical optimizations were performed at the Density Functional Theory (DFT) level. The B3LYP [26, 27] exchange-correlation functional and the base set def2-TZVP [28] were used. All calculations were performed by Gaussian 16 [29]. In the DFT calculations, geometry optimizations, including hydrogen atoms, were performed without any symmetry constraint.

Results and discussion

The DMSO solvate of 1

The DMSO solvate of 1 was solved in the non-centrosymmetric orthorhombic space group $P2_12_12_1$ with one calixarene molecule and three DMSO ones in the asymmetric unit. Calixarene adopts a classical cone conformation with hydrogen bonds between the hydroxyl groups

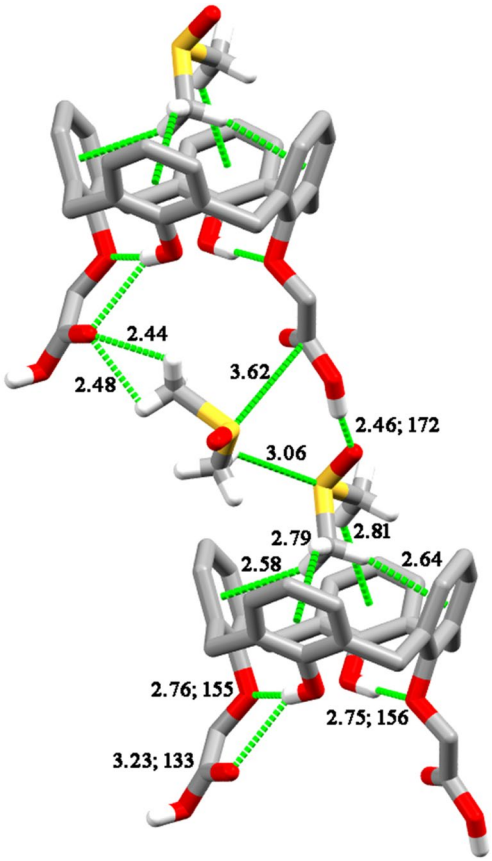

Fig. 1 The DMSO solvate of **1** elucidated here. Most of the hydrogens were omitted to clarity (except OH and DMSO ones). For CH…π and CH…O interactions, the distances are calculated between the hydrogen and the entire phenyl centroid. For classical hydrogen bonds, the O…O distance (in Å) and the OH…O angle (in °) are shown. The distance 3.62 Å was measured between sulfur and the carbonyl carbon

and the oxygen atoms of carboxymethyl. One DMSO is strongly entrapped inside the crown, performing CH…π interactions with phenyl rings (Fig. 1). This same DMSO is a hydrogen bonding acceptor from the carboxyl group of another calix [4] arene molecule packed along the *b* axis. Another crystallographically independent DMSO molecule is positioned between the two carboxymethyl legs of the same calix [4] arene, interacting by means of the sulfur electron lone pair with one carboxyl group and through its methyl group with another CO_2H moiety (Fig. 1). Finally, the third DMSO in the asymmetric units is a non-classical hydrogen bonding donor to hydroxyl and carbonyl oxygens of the same calix[*n*]arene molecule. Compound 1 has already been elucidated in the solid state, exhibiting the same cone conformation in metal-free crystal forms [hydrate (Cambridge Structural Database (CSD) reference code CEFWAM), acetone solvate (UFIQEG), 1,10-phenanthroline tetrahydrofuran solvate (MITKAE), and chlorhexidinium monohydrate (WODGIG)].

The calcium salt of 2

The other calix [4]arene has also adopted cone conformation in the new crystal form reported here. Compound 2 is tetra-sulfonated in its upper rim, with intact hydroxyl groups at the lower rim. It has been well studied in the solid state, with 320 entries in the CSD (version 6.01, November 2025) [30]. Of these 320 structures, there is only one that differs from the cone conformation (CSD reference code BUCRIA, 1,3-alternate conformation). Here, there is one calix [4]arene molecule in the asymmetric unit solved in the centrosymmetric monoclinic space group $P2_1/n$, with three sulfonic groups deprotonated and bonded to two crystallographically calcium ions (one with full occupancy, Ca1, and another one with half occupancy on an inversion center, Ca2). The protonated sulfonic group does not bind to calcium and is a hydrogen bonding donor to hydroxyl oxygen of another calix [4]arene molecule packed along the [101] direction (Fig. 2). This interaction is responsible for connecting molecular sheets along the *b* axis (see below). In addition, in the asymmetric unit, there are five water molecules bonded to full occupancy calcium and another one bonded to half occupancy calcium, in addition to two ethanol molecules and two water not interacting with calcium. Ca1 and Ca2 adopt pentagonal and square bipyramid geometries, respectively, keeping the calix [4]arene molecules in contact in two-dimensions (along the *c* and *a* axes, by Ca1 and Ca2, respectively), giving rise to molecular sheets made up of cross-linked calcium and calixarene species (Fig. 2). In the same way as seen in compound 1, one solvent molecule is strongly entrapped inside the crown. This ethanol molecule interacts with phenyl rings through its hydroxyl and methyl groups, while methylene moiety is a non-classical hydrogen bonding donor to SO_3^- of another calix [4]arene packed along the *b* axis. A similar orientation of calixarenes molecules is found in another literature crystal structure of this compound (YENQIR), which is present even without metal ion and cocrystallized with a larger guest (1,4,8,11-tetra-azoniocyclotetradecane). Ten crystal forms thereof with ethanol are known (HUVXUV, ICOYAC, OROXID, OROYIE, WOXLAY, OROXUP, RADGOT, RADHAG, RADHEK, YOFBII), in which the first five codes have ethanol included inside the crown, as occurs in our structure. One precedent with calcium is also existent (YAYLOB), with 2,2'-bipyridine also bonded to calcium ions and included inside the crown.

The two polymorphs of 3, including DFT calculations

Here, the crystal structure of compound 3 is elucidated for the first time in two true conformational polymorphs, both crystallizing in the centrosymmetric triclinic space group *P*-1.

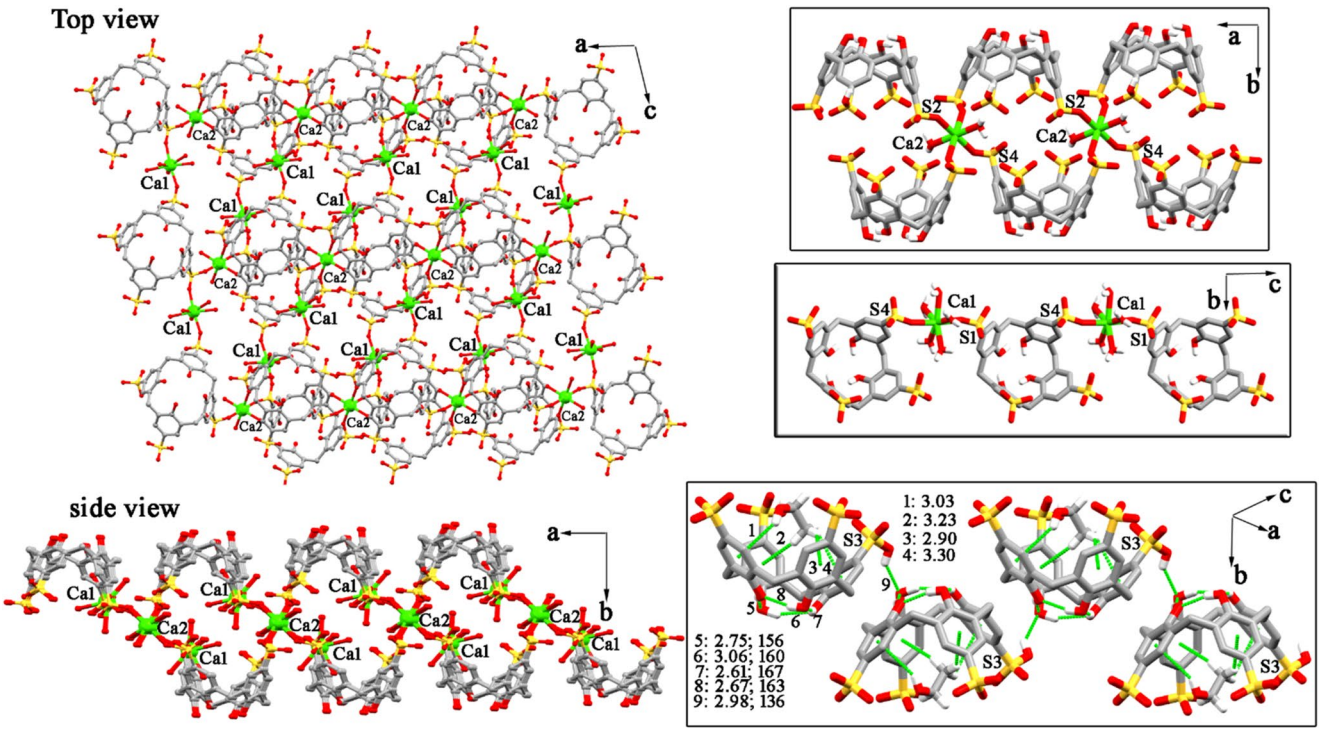

Fig. 2 The calcium-calixarene sheets formed in the crystal form of 2 elucidated here. Most of the hydrogens were omitted for clarity (except OH and ethanol ones in the framed panels). For CH…π and OH…π interactions, the distances are calculated between the hydrogen and the entire phenyl centroid. For classical hydrogen bonds, the O…O distance (in Å) and the OH…O angle (in °) are shown

Two molecular halves rise into two entire calixarene molecules by the inversion symmetry present in the crown centers (Fig. 3). Both polymorphs have general 1,2,3-alternate [31] conformations as well as in the ethyl ester analog. However, in the literature related crystal structure (CSD reference code DAKSIR), two ethyl ester legs are pointed inward the crown center, and carbonyl oxygen atoms point toward themselves in the cavity center. In one of our polymorphs, labeled as Form I, and in one molecule of the so-called Form II, this conformation is similar, but carbonyl oxygens point outwards the cavity, laying out the OCH_3 moieties in the cavity center. In one molecule of Form I (labeled as B), this former group is disordered over two site sets of equal occupancy (parts A and B). The orientation of the carbonyl and the alkyl ester groups found in the ethyl ester analog occurs in this part B. Anyway, to adopt this conformation, in our compound and in the literature analog, the phenyl rings having the ester legs pointed inwards the cavity center are tilted outwards the cone [with angles relative to the plane calculated through the six methylene carbons of the crown measuring 32.8° and 44.6° in Form I (molecules A and B, respectively) and 44.4° in Form II (molecule A)], while the four neighboring phenyl rings incline inwards the cone [with corresponding crystallographically independent angles of 59.3°/83.9° and 69.2°/73.8° in Form I (molecules A and B, respectively) and 68.7°/84.7° in Form II (molecule A)].

As stated, the two molecules of Form I are formed with its two crystallographically independent molecular halves. Although they are similar, they are not equal. If disordered methyl sites that point to the center of the cavity of molecule B are considered, the root-mean square deviation (RMSD) for their superimposed non-hydrogen atoms is greater than 1 Å, and there are different patterns of CH…π interactions inside the crown. Most of these interactions are localized on two phenyl carbons and are related to different conformations of the methyl ester legs inside the crown. Molecule A has these legs inclined out of the meridional plane crossing the crown, pointing in the direction of an inner side of the crown, while these legs are more aligned with the center of the cavity in molecule B. The torsion around O-CH_2 bond connecting the methylene moiety to phenolate oxygen describes this leg conformation. It measures 140.9(7)° and 156.3(7)° in molecules A and B of Form I, and 140.1(4)° in molecule A of Form II, which, however, has more overall resemblance with molecule B of Form I given their lowest RMSD value (Fig. 3). In contrast to these three resembled molecules, the other one (molecule B) has a different 1,2,3-cone conformation in Form II, that is marked by cavity closing through strong inclination of two inversion symmetry related phenyl rings inwards the cavity center instead of methyl ester legs. These phenyl rings form an angle of 32.3° with the plane formed with the methylene carbons of the

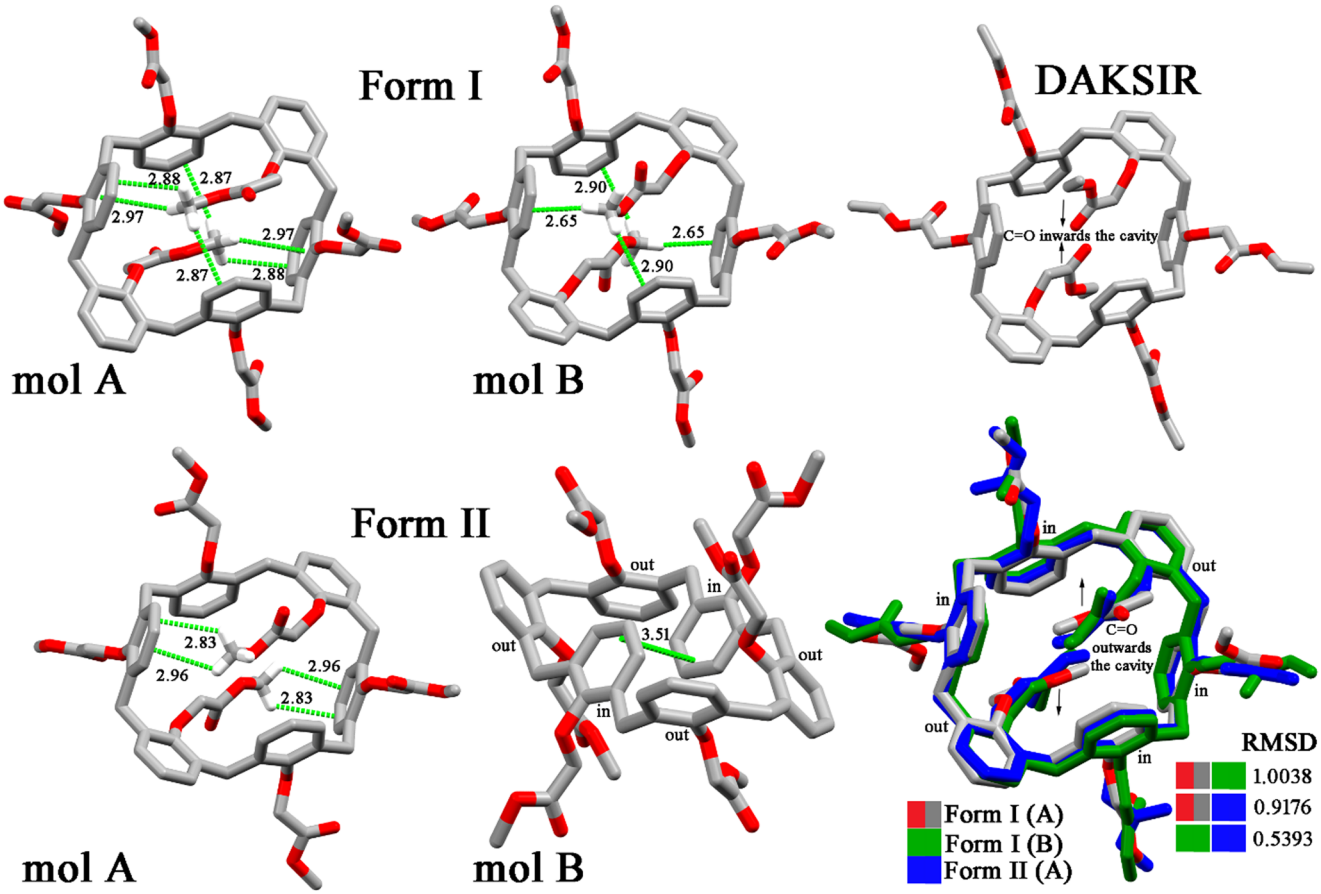

Fig. 3 The molecules of 3 in its two polymorphs elucidated here, and its ethyl ester analog (CSD reference code DAKSIR). Only part A of molecule B is shown for Form I (part B can be seen in the next picture). Hydrogens were hidden for sake of clarity (except those of methyl groups pointed inwards the crown cavity). The distances are calculated between the hydrogen and the interacted bond centroid (except for those measuring 2.97 Å, that is the entire phenyl centroid, and 3.51 Å, that is between the centroids calculated through the 3,4,5-carbons). The phenyl inclination inwards or outwards the cavity center is also depicted together with carbonyl orientation relative to the cavity center. In the overlay picture, molecule A of Form I was used as pivot to superimpose the two others, and the root mean square deviation (RMSD) values for the superimposed atoms are in Å

crown. In turn, the other four phenyl rings are bent outwards the cone, with two angles of 61.1° and two others of 62.8° (Fig. 3).

In order to get insights on the conformations adopted by 3 in its two polymorphs, we have entered their coordinates into the DFT calculations of energy and geometry optimization. The optimized conformations were well fitted to the experimental ones, as can be viewed in all RMSD values being lower than 1.0 Å (Fig. 4). Moreover, the lowest energy conformation came from molecule A of Form I, which had the highest RMSD value (0.9044 Å) between experimental and theoretical geometries. This energy lowering and geometry deviation increase in the optimized conformation received contribution from moving the methyl ester legs from the cavity center towards the neighboring legs, setting them closer to each other so that CH moieties can be brought together with the oxygen atoms. Another interesting finding resides in the low relative energy for molecule B of Form I with carbonyl group pointing inward the cavity center as occurs in the ethyl ester analog (DAKSIR reference code). This conformation, labeled part B of molecule B, would have at room temperature (298 K) a population of ca. 23% of that of the lowest energy conformer, while the populations of its part A and molecule A of Form I do not reach 8% of the minimal energy population in this temperature. However, for the atypical conformer B of Form II, the corresponding population is around 10^{-5}%, evidencing its very high-energy and the difficult task of isolating this polymorph. Nevertheless, the isolation of this polymorph is possible due to contributions from intermolecular interactions and solvation energies.

Crystal forms of *p-tert*-butylcalix[8]arenes 4 and 5

Another compound crystallographically elucidated here is 4 (triclinic, *P*-1). It adopts a cone conformation with an alternate pattern of phenyl ring inclination, clearly enclosing the

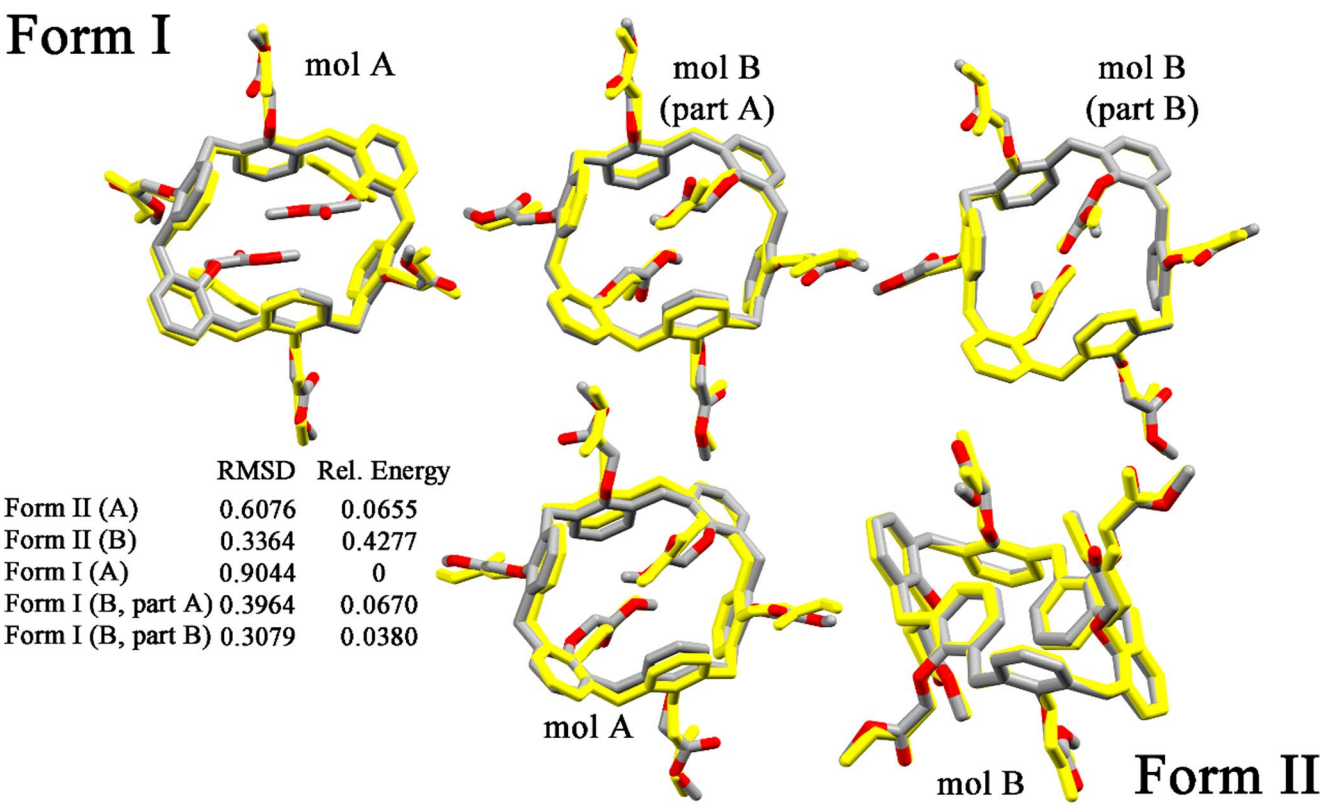

Fig. 4 Molecular overlay between each conformation found in the two polymorphs of 3 (sticks colored by element) and the corresponding DFT-optimized molecules (yellow sticks). The RMSD values for the superimposed atoms are in Å, and the relative energies are in eV

crown entry with four *t*-butyl substituted aromatic heads (Fig. 5). This conformational pattern can be viewed in the angles between phenyl rings and the plane calculated through the eight methylene carbons, which, in alternance, assume similar values (in sequence these angles measure 54.3° (out), 59.3° (in), 55.3° (out), 62.0° (in), 51.5° (out), 64.5° (in), 47.7° (out) and 68.3° (in)). In the lower rim, one *n*-butyl chain is directed inward to the center of the cavity, making no interaction with the guest there. This conformation is similar to that found in the calix [8]arene with *t*-butyl on the upper rim and the carboxymethyl ethyl ester on the lower rim (CSD reference code MADHOP).

A new crystal form of *p-tert*-butylcalix [8]arene (5) was synthesized and solved by single-crystal X-ray diffraction. It has crystalized in the triclinic space group *P*-1 with two crystallographically calix [8]arene molecules adopting the pleated-loop conformation, which is common in solvated crystal structures of this compound [32]. These molecules resemble (Fig. 6), while their packing patterns differ. Indeed, this is the first report with Z'>1 for *p-tert*-butylcalix [8]arene. While one molecule exhibits a chain of stacked inversion-symmetry related units, growing along the *a* axis, another crystallographically independent molecule forms

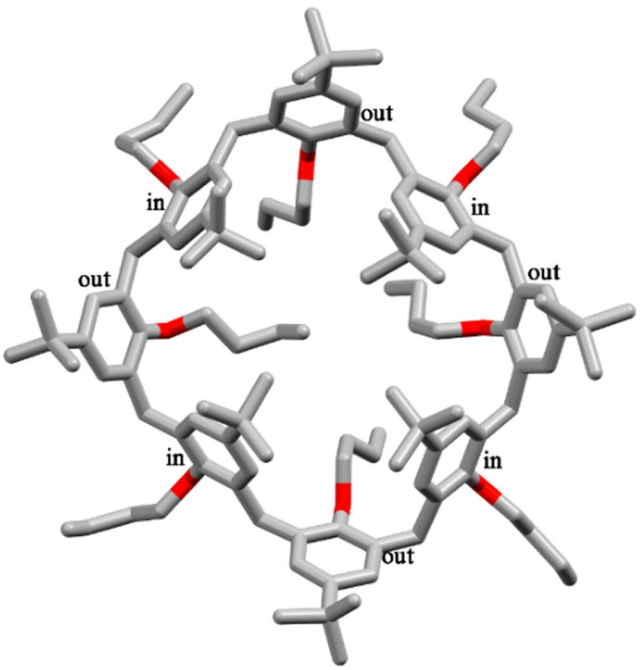

Fig. 5 The asymmetric unit of compound 4. The phenyl inclination inwards or outwards the cavity center is depicted (hydrogens were hidden for clarity)

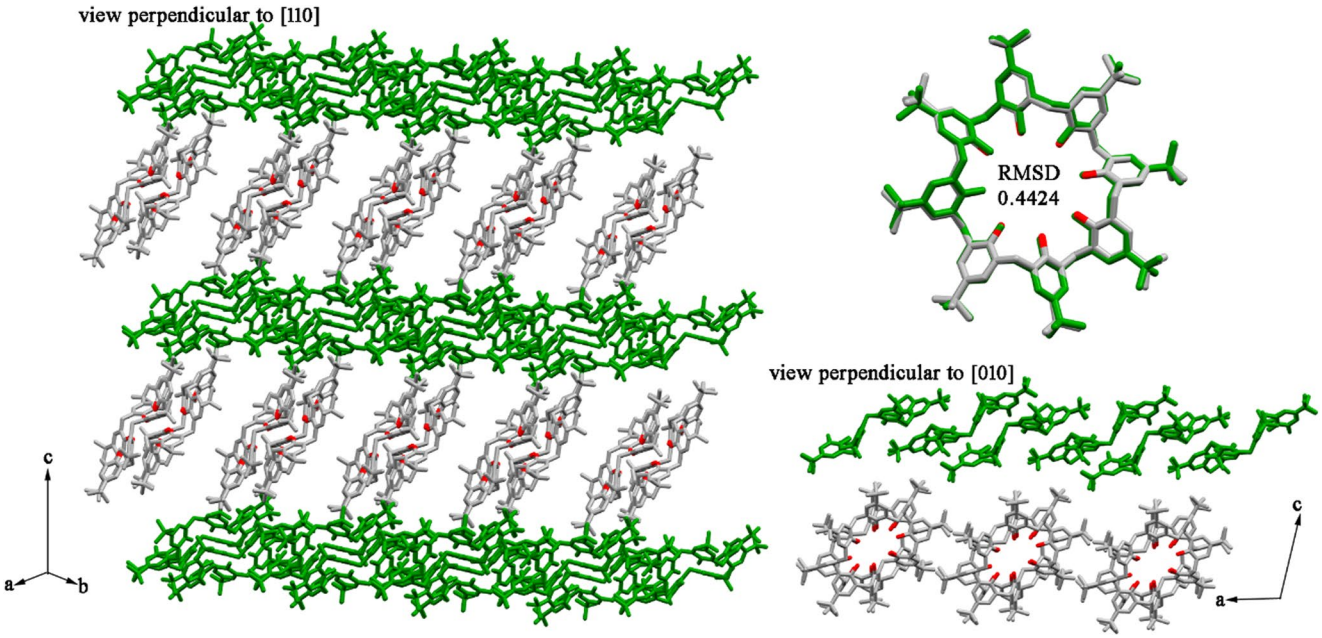

Fig. 6 The conformational similarity between the two crystallographically independent molecules of 5 contrasts with their different packing motifs. In all pictures, molecules labeled as A and B are by-element and green colored, respectively (hydrogens were hidden for clarity). In the left view, the spaces between the dimers of molecules A are filled with solvent molecules

centrosymmetric dimers which are separated away by solvent channels. Both packing motifs are found in other solvated crystal structures of *p-tert*-butylcalix [8]arene [32], but not simultaneously in the same architecture as found here.

Hirshfeld surface analysis

The Hirsfeld surface was computed to further inspect intermolecular interactions in our structures, most of which have only weak interactions in their crystal lattice. Hirshfeld surface for our structure of 5 is featured by short side wings and one central short spike accompanied by almost whole body, corresponding to C…H (12.6%) and H…H (84.6%) interactions (Fig. 7). When computed individually for each molecule, the Hirshfeld surface analysis reveals that molecule B has a higher proportion of H…C interactions assembling the chains (14.4% against 9.0% in molecule A), whereas the H…H interactions are more abundant in the dimers of A (89.2% over 82.1% in molecule B). The C…C interactions typical of π…π interactions are very low in both molecules (0.4% in A and 0.5% in B). This pattern of interactions distribution is similar in compound 4, whose Hirshfeld surface is present mainly with H…H (88.3%) and C…H (8.9%) interactions (Fig. 7), without any contribution of C…C interactions.

Polymorphism of compound 3 can be also assigned by Hirshfeld surface analysis. The Hirshfeld surface fingerprint shapes differ for their polymorphs. This map of Form II has two sharper spikes referring to O…H interactions, which are slightly more abundant in this polymorph (28.3% against 25.0% in Form I). The Form II fingerprint has also a central elongated and bifurcated tip, referring to H…H interactions, while these interactions outline a shorter central tip with two side broader spikes in Form I (Fig. 8). However, the Hirshfeld surface computed individually for each of the two molecules present in each polymorph does not show significant differences (Fig. 8).

Unlike the structures of compounds 3–5 reported here, Hirshfeld surface fingerprints of 1 and 2 in the crystal forms elucidated here exhibit the occurrence of classical OH…O hydrogen bonds (Fig. 9). For the DMSO solvate of 1, very sharp symmetric spikes are found, with the upper and lower spikes corresponding to hydrogen donor and acceptor groups, respectively. Their end dots have short *di* and *de* distances at ∼0.6 Å or at ∼0.9 Å, reflecting the strong classical OH…O hydrogen bond between calixarene and DMSO molecules (Figs. 1 and 9). For the calcium salt of 2, the hydrogen bonding spikes are also viewed in its Hirshfeld surface fingerprint, with short ending (di, de) pairs around 0.7 Å and 1.1 Å, indicating the presence of strong OH…O bonds as described earlier (Figs. 2 and 9). In this structure, these interactions are even the most abundant, contributing to 42.9% of the total points of the surface.

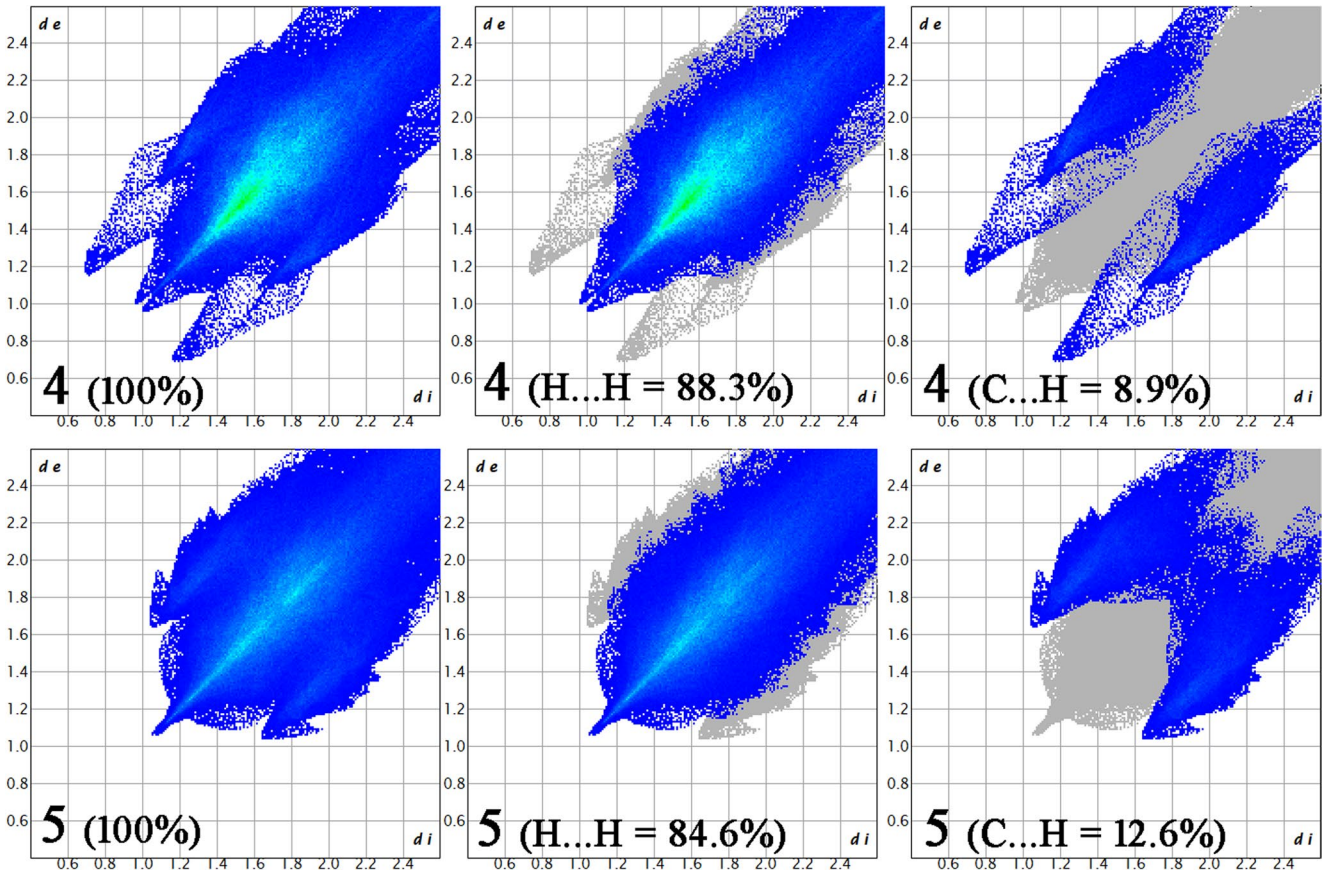

Fig. 7 Full fingerprint maps of the Hirshfeld surface and the major interactions contributions calculated for the structures of 4 and 5 elucidated here. Here and in the next two figures, the blue color indicates lower proportions of a (d_i,d_e) pair; green outlines an intermediary frequency; and red draws an upper limit fraction greater than 0.1% of the surface points with the same (d_i,d_e) combination. Gray shadow draws the distances of the interactions hidden in the panel

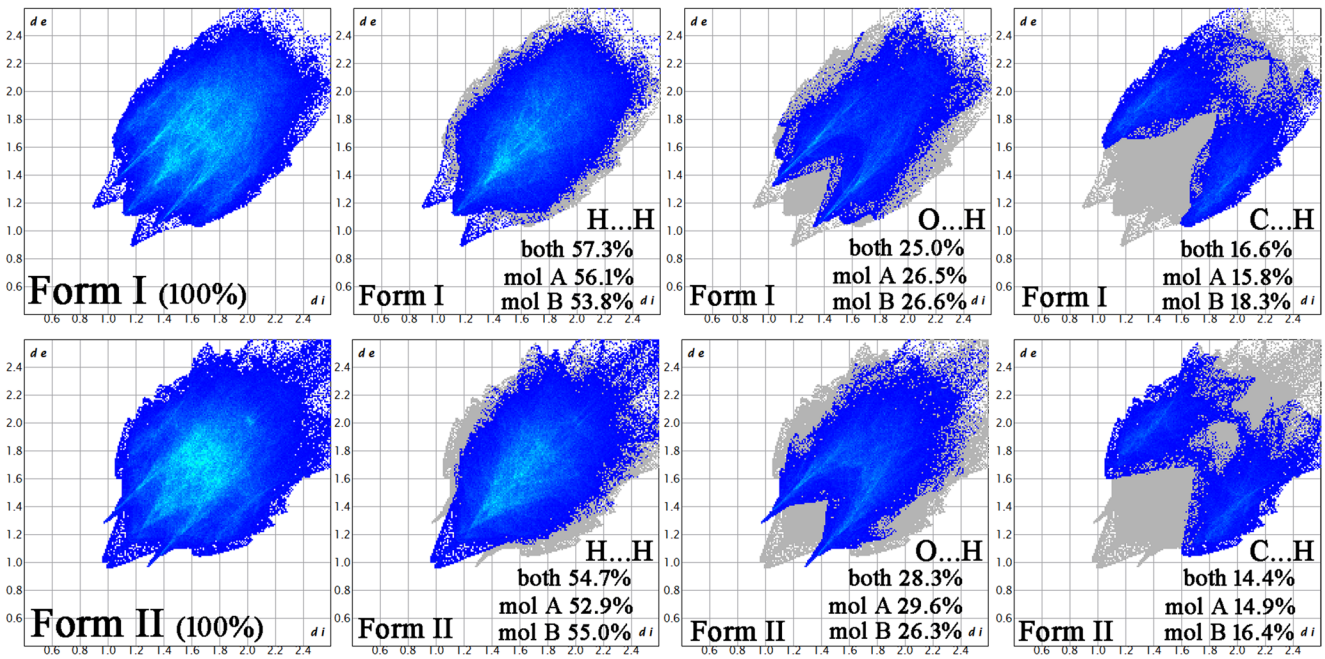

Fig. 8 Polymorphism ascribing in compound **3** by Hirshfeld surface analysis. Surface were calculated for both molecules of each polymorph and by selecting only one molecule at a time. For more guidance, see Fig. 7 caption

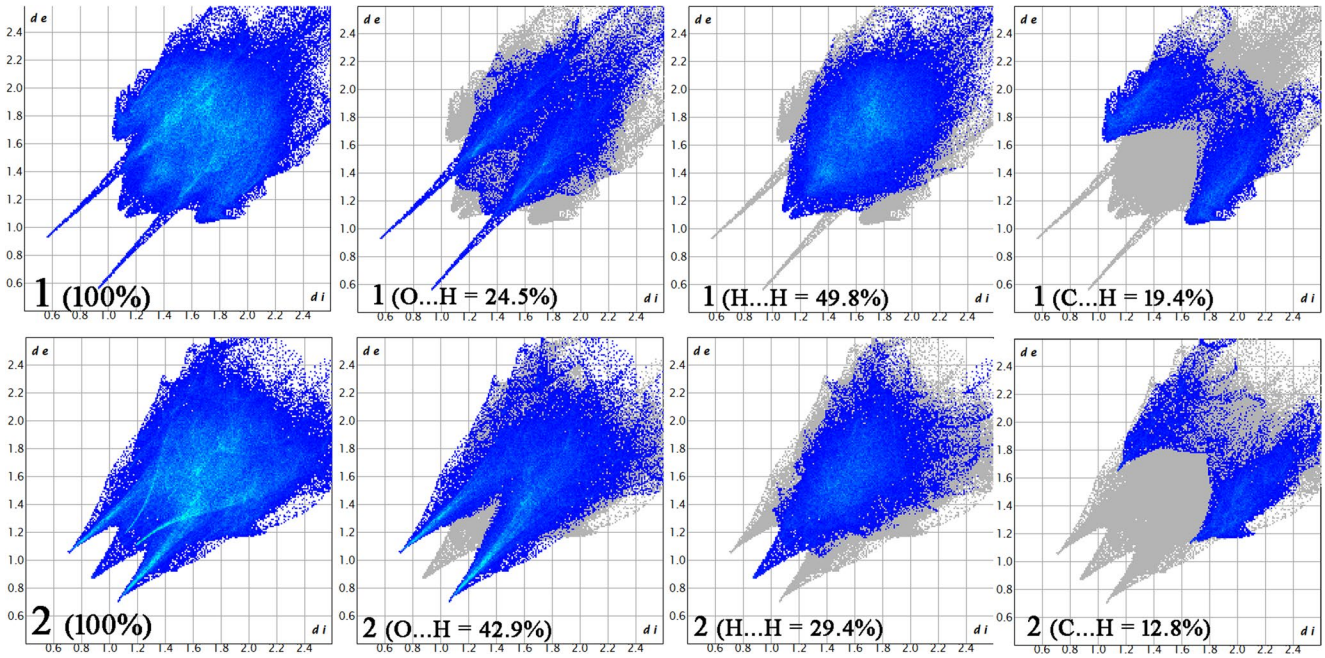

Fig. 9 Classical OH…O hydrogen bonds viewed in the Hirshfeld surface fingerprints for the crystal forms of 1 and 2 elucidated here. For guidance, see Fig. 7 caption

Conclusion

The results presented here expanded the actual knowledge on the crystal forms and conformations of calix[*n*]arenes (*n* = 4, 6 or 8). The solved structures of calix [4]arenes reinforce their trend to work as hosts due to their open cavity, while the elucidation of the calix [6]arene shows that its cavity is filled by itself in both isolated polymorphs, which exhibited typical conformerism to close the crown cavity. Surprisingly, a high-energy conformer was found in one of its polymorphs, which also keeps the crown closed by the π…π interaction between phenyl rings. This conformational propensity to not expose the cavity to guests was also observed in the *p-tert*-butylcalix [8]arene substituted with *n*-butyl at lower rim, while the calix [8]arene without this lower rim functionalization was crystallized with similar molecules showing different packing motifs. The findings of this study can contribute to a better understanding of the (un)success of host-guest supramolecular strategies for similar and related compounds, allowing more accurate efforts to be made towards smart multicomponent aggregates made up of calixarenes. Notably, the results indicate that the calix [4]arenes have higher chance to receive guests inside their crown in the solid state, when, for instance, they are conceived into a host-guest approach to improve drug delivery performance, while functionalization on the lower rim should be avoided in the calix[*n*]arenes (*n* = 6, 8) whether this is desired.

Supplementary Information The online version contains supplementary material available at https://doi.org/10.1007/s11224-026-02834-1.

Author contributions All authors contributed to the study conception and design. Data collection was performed by M.A.M.L., M.E.A., G.M.F. and B.J.G.D. Data analysis and interpretation were performed by F.F.G., A.F., C.M.S. and F.T.M. Figures preparation was performed by C.M.S and F.T.M. The first draft of the manuscript was written by F.T.M. and all authors commented on previous versions of the manuscript. All authors read and approved the final manuscript.

Funding The Article Processing Charge (APC) for the publication of this research was funded by the Coordenação de Aperfeiçoamento de Pessoal de Nível Superior - Brasil (CAPES) (ROR identifier: 00x0ma614). The authors acknowledge Financiadora de Estudos e Projetos (FINEP/Brazil; Agreement UFMG/FINEP #0245/24), Ministério da Ciência, Tecnologia e Inovações (MCTI/Brazil), Conselho Nacional de Desenvolvimento Científico e Tecnológico (CNPq/Brazil; Grants 313114/2021-8, 406744/2022-0, 307074/2023-4, 309922/2023-2, 403474/2025-6 and 305243/2026-8), Coordenação de Aperfeiçoamento de Pessoal de Nível Superior (CAPES/Brazil - Finance Code 001), Fundação de Amparo à Pesquisa do Estado de Minas Gerais (FAPEMIG/Brazil; Grants # APQ-04111-24, APQ-00475-25, APQ-00865-26 and RED-00082-23), Secretaria de Estado de Desenvolvimento Econômico de Minas Gerais (SEDE-MG/Brazil), Secretaria de Estado de Saúde de Minas Gerais (SES-MG/Brazil) and amendments by the representatives of the Brazilian states or of the federation of Brazil. ADF, CMS and FTM are recipient of research fellowship from CNPq/Brazil.

Data availability The datasets generated during the current study are available in the Cambridge Structural Database (CSD) repository.

Declarations

Ethics approval Not applicable.

Competing interests The authors declare no competing interests.

References

1. Ferreri L, Granata G, Forte G, Cervello M, Cusimano A, Petralia S, Consoli GML (2026) Calixarene-based nanostructures for delivering coumarin 6 for tumor-cell imaging and photoinduced toxicity. ACS Appl Nano Mater 9(10):4493–4503. https://doi.org/10.1021/acsanm.5c05263
2. Abdulla HM, Sajith PK, Khire SS, Remya K (2026) Host-guest interaction of NO and NO^+ species with calixerenes: dissecting the impact of conformational and confinement effects. Phys Chem Chem Phys 28(5):3562–3575. https://doi.org/10.1039/d5cp03650j
3. Chen X, Xu P, Wang Q, Hui W, Fan B, Song L, Xu XP, Wu YH, Peng Q (2025) Supramolecular cavity confinement inducing ordered C60 assembly and suppressed interfacial non-radiative recombination for efficient and scalable perovskite solar cells. Adv Funct Mater e30794. https://doi.org/10.1002/adfm.202530794
4. Pan YC, Li JX, Guo DS (2025) The rise and promise of macrocyclic hosts in biomedicine. ACS Cent Sci 11(12):2304–2318. https://doi.org/10.1021/acscentsci.5c00891
5. Rebek J Jr (2000) Host-guest chemistry of calixarene capsules. Chem Commun 8:637–643. https://doi.org/10.1039/a910339m
6. Martins FT, Da Silva CM, Vasconcelos GA, Gontijo Vaz B, Vieira TDS, Queiroz Júnior LHK, De Fátima (2016) Â Lower rim dimerization of a calixarene through the encapsulation of sodium ions. CrystEngComm 18:6987–6991. https://doi.org/10.1039/C6CE01387B
7. Alvarenga ME, Mendes NSR, Parreira G, Marreto RN, Da Silva CM, De Fátima Â, Silva FA, Martins FT (2025) A calix[4]tube-resveratrol cocrystal improving the nutraceutical solubility in water. J Mol Struct 1322(1):140–217. https://doi.org/10.1016/j.molstruc.2024.140217
8. Řezanková M, Budka J, Mikšátko J, Eigner V, Císařová I, Cuřínová P, Lhoták P (2017) Anion receptors based on intramolecularly bridged calix[4]arenes bearing ureido functions. Tetrahedron 73:742–749. https://doi.org/10.1016/j.tet.2016.12.054
9. Kumar R, Sharma A, Singh H, Suating P, Kim HS, Sunwoo K, Shim I, Gibb BC, Kim JS (2019) Revisiting fluorescent calixarenes: from molecular sensors to smart materials. Chem Rev 119(16):9657–9721. https://doi.org/10.1021/acs.chemrev.8b00605
10. Nag R, Rao CP (2022) Calixarene-mediated host-guest interactions leading to supramolecular assemblies: visualization by microscopy. Chem Commun 58(41):6044–6063. https://doi.org/10.1039/d2cc01850k
11. Muley S, Dhila H, Gote M (2024) Calixarene-guest complexes: the next innovation in delivery of drugs and biologics. Adv Th 7(10):2400207. https://doi.org/10.1002/adtp.202400
12. Furer VL, Vandyukov AE, Ovsyannikov AS, Strelnikova IV, Agarkov AS, Solovieva SE, Antipin IS (2024) Study of the structure of 1,3-disubstituted thiacalix[4]arenes with phthalimide and imine groups using vibrational and NMR spectroscopy. Struct Chem 35:1479–1491. https://doi.org/10.1007/s11224-024-02298-1
13. Gabdulkhaev MN, Ziganshin MA, Gubaidullin AT, Gorbachuk VV (2023) Reproducible preparation of polymorphs of the thiacalix[4]arene derivative by saturating a solid host with solvent vapors. J Struct Chem 64(11):2040–2050. https://doi.org/10.1134/S0022476623110021
14. Gataullina KV, Ziganshin MA, Stoikov II, Klimovitskii AE, Gubaidullin AT, Suwinska K, Gorbatchuk VV (2017) Smart polymorphism of thiacalix[4]arene with long-chain amide containing substituents. Cryst Growth Des 17:3512–3527. https://doi.org/10.1021/acs.cgd.7b00463
15. Gabdulkhaev MN, Ziganshin MA, Buzyurov A, Schick C, Solovieva SE, Popova E, Gubaidullin AT, Gorbatchuk VV (2020) Smart control of calixarene polymorphic states. CrystEngComm 22:7002–7015. https://doi.org/10.1039/d0ce01070g. rsc.li/crystengcomm
16. Santos FM, Souza PC, Neto JAN, Valdo AKSM, Ribeiro L, Guedes GP, Silva CM, De Fátima Ã, Martins FT (2019) Inter and intra-phase conformerism in two calix[4]arenes. J Mol Struct 1198:126849. https://doi.org/10.1016/j.molstruc.2019.07.096
17. da Silva DL, Fernandes SA, Sabino AA, de Fátima Â (2011) p-Sulfonic acid calixarenes as efficient and reusable organocatalysts for the synthesis of 3, 4-dihydropyrimidin-2 (1H)-ones/-thiones. Tetrahedron Lett 52(48):6328–6330. https://doi.org/10.1016/j.tetlet.2011.08.175
18. Neto LS, Maia AFS, Godin AM, Augusto PSA, Pereira RLG, Caligiorne SM, Alves RB, Fernandes SOA, Cardoso VN, Goulart GAC, Martins FT, das Neves MCL, Garcia FD, de Fátima Â (2022) Calix[n]arene-based immunogens: A new non-proteic strategy for anti-cocaine vaccine. J Adv Res 38:285–298. https://doi.org/10.1016/j.jare.2021.09.003
19. SADABS, APEX2 and, Bruker SAINT (2009) AXS Inc., Madison, Wisconsin, USA
20. Sheldrick GM (2015) Crystal structure refinement with SHELXL. Acta Cryst 71:3–8. https://doi.org/10.1107/S2053229614024218
21. Dolomanov OV, Bourhis LJ, Gildea RJ, Howard JAK, Puschmann H (2009) OLEX2: a complete structure solution, refinement and analysis program. J Appl Cryst 42:339–341. https://doi.org/10.1107/S0021889808042726
22. Macrae CF, Sovago I, Cottrell SJ, Galek PTA, McCabe P, Pidcock E, Platings M, Shields GP, Stevens JS, Towler M, Wood PA (2020) Mercury 4.0: from Visualization to Analysis, Design and Prediction. J Appl Cryst 53:226–235. https://doi.org/10.1107/S1600576719014092
23. Atwood JL, Barbour LJ, Jerga A (2002) Storage of Methane and Freon by Interstitial van der Waals Confinement. Science 296:2367–2369. https://doi.org/10.1126/science.1072252
24. Spackman MA, Jayatilaka D (2009) Hirshfeld surface analysis. CrystEngComm 11:19–32. https://doi.org/10.1039/B818330A
25. Spackman PR, Turner MJ, McKinnon JJ, Wolff SK, Grimwood DJ, Jayatilaka D, Spackman MA (2021) Crystal Explorer: a program for Hirshfeld surface analysis, visualization and quantitative analysis of molecular crystals. J Appl Crystallogr 54:1006–1011. https://doi.org/10.1107/S1600576721002910
26. Stephens PJ, Devlin FJ, Chabalowski CF, Frisch MJ (1994) Ab initio calculation of vibrational absorption and circular dichroism spectra using density functional force fields. J Phys Chem 98:11623–11627. https://doi.org/10.1021/j100096a001
27. Becke AD (1993) Density-functional thermochemistry. III. The role of exact exchange. J Chem Phys 98:5648–5652. https://doi.org/10.1063/1.464913

28. Weigend F, Ahlrichs R (2005) Balanced basis sets of split valence, triple zeta valence and quadruple zeta valence quality for H to Rn: design and assessment of accuracy. Phys Chem Chem Phys 7:3297–3305. https://doi.org/10.1039/B508541A
29. Frisch MJ, Trucks GW, Schlegel HB, Scuseria GE, Robb MA, Cheeseman JR, Scalmani G, Barone V, Petersson GA, Nakatsuji H, Li X, Caricato M, Marenich AV, Bloino J, Janesko BG, Gomperts R, Mennucci B, Hratchian HP, Ortiz JV, Izmaylov AF, Sonnenberg JL, Williams-Young D, Ding F, Lipparini F, Egidi F, Goings J, Peng B, Petrone A, Henderson T, Ranasinghe D, Zakrzewski VG, Gao J, Rega N, Zheng G, Liang W, Hada M, Ehara M, Toyota K, Fukuda R, Hasegawa J, Ishida M, Nakajima T, Honda Y, Kitao O, Nakai H, Vreven T, Throssell K, Montgomery JA Jr, Peralta JE, Ogliaro F, Bearpark MJ, Heyd JJ, Brothers EN, Kudin KN, Staroverov VN, Keith TA, Kobayashi R, Normand J, Raghavachari K, Rendell AP, Burant JC, Iyengar SS, Tomasi J, Cossi M, Millam JM, Klene M, Adamo C, Cammi R, Ochterski JW, Martin RL, Morokuma K, Farkas O, Foresman JB, Fox DJ (2016) Gaussian 16 Revision B.01, Gaussian Inc., Wallingford CT.
30. Groom CR, Bruno IJ, Lightfoot MP, Ward SC (2016) The Cambridge Structural Database. Acta Cryst Sect B 72:171–179. https://doi.org/10.1107/S2052520616003954
31. Choe JI, Kim K, Chang SK (2000) Computer simulations on molecular recognition of alkylamines by ester derivatives of p-tert-butylcalix[6]arene. Bull Korean Chem Soc 21:200–206
32. Kieliszek A, Malinska M (2021) Conformations of p-tert-butylcalix[8]arene in solvated crystal structures. Cryst Growth Des 21. https://doi.org/10.1021/acs.cgd.1c00773. :6862 – 6871